Journal of the European Ceramic Society 22 (2002) 2061–2070

www.elsevier.com/locate/jeurceramsoc

Mechanical properties of gas pressure sintered Si_3N_4/SiC nanocomposites

Petra Rendtel[1], Andreas Rendtel*[,2], Heinz Hübner

Technical University Hamburg-Harburg, Materials Science and Technology Group, D-21071 Hamburg, Germany

Received 8 June 2001; received in revised form 15 November 2001; accepted 8 December 2001

Abstract

The mechanical properties of gas pressure sintered Si_3N_4/SiC nanocomposite materials were studied at room temperature and in the range of 1400–1600 °C. Fracture strength at room temperature was found to be between 640 and 840 MPa and thus within the range of data reported in the literature for other gas pressure sintered silicon nitride ceramics. At elevated temperature the creep and stress rupture behaviour were determined in four-point bending. The creep behaviour is characterised by primary and pronounced secondary creep, very high activation energies for creep in the range of 1050–1450 kJ/mol, and two different stress dependencies. At stresses below a characteristic transition stress in the range 170–200 MPa the stress dependency is described by a stress exponent of around two. Above the transition stress, stress rupture was observed to be controlled by subcritical crack growth with stress rupture exponents of 30–40. Annealing of the as-sintered materials promotes crystallisation of the intergranular glassy phase resulting in an increase in creep strength and resistance against subcritical crack growth. An extensive analysis of the available literature data revealed that the materials tested in this study belong to the most creep resistant silicon nitride ceramics prepared by gas pressure sintering. © 2002 Published by Elsevier Science Ltd.

Keywords: Composites; Creep; Gas pressure sintering; Mechanical properties; Si_3N_4; Si_3N_4–SiC

1. Introduction

Ceramic matrix composites reinforced by nano- or submicron-sized SiC particles are structural materials with promising high temperature properties. In the late 80′s Niihara proposed the nanocomposite concept.[1] According to this concept it is thought that the addition of nano-sized particles to a ceramic matrix improves the mechanical properties of the material. Since that time various investigations were carried out to verify the nanocomposite concept for silicon nitride based ceramics.[2–4] Simultaneously, the preparation methods of such materials were improved.[5,6] Many of the results emphasised Si_3N_4/SiC composites as the leading material for high temperature applications. Ceramics of this type are characterised by very low creep rates even above 1400 °C[4] and an improved oxidation resistance.[7] It became evident that materials with advanced mechanical properties were only obtained if the preparation process was controlled properly and the optimal process parameters were known.[5,6]

So far, most of the Si_3N_4/SiC nanocomposites were produced by hot pressing (HP). It was found that densification is hindered by the added SiC particles.[6,8] This is of less importance for the densification by HP, where a slightly higher densification temperature is sufficient to overcome this problem. But, densification by pressureless sintering (PLS) or gas pressure sintering (GPS) is much more complicated.[9] On the other hand, GPS has the advantage to allow the production of a broad variety of possible shapes. In several investigations the densification problem arising with GPS was solved by using relatively large amounts of sintering additives, in particular mixtures of yttria and alumina or silica.[5,9] During sintering these additives form a large amount of liquid phase leading to a pronounced densification of the material. On the other hand, on cooling this liquid gives a large amount of amorphous phase at the grain boundaries due to limited crystallisation.[10,11] This amorphous phase has a low softening temperature and

* Corresponding author at present address.
E-mail address: Andreas.Rendtel@wacker.com (A. Rendtel).
[1] Now with Krüss GmbH, Hamburg, Germany.
[2] Present address: Wacker-Chemie GmbH, Max-Schaidhauf-Str 25, D-87437 Kempten, Germany.

0955-2219/02/$ - see front matter © 2002 Published by Elsevier Science Ltd.
PII: S0955-2219(01)00526-X

hence the high temperature properties deteriorate. It was shown by Herrmann et al.[6] that it is possible to prepare Si_3N_4/SiC nanocomposites with Y_2O_3 as the only additive by GPS. Recent results also showed that the high temperature properties of silicon nitride doped with yttria only are remarkably improved.[4]

In the present study high temperature properties of Si_3N_4/SiC nanocomposites were investigated. The materials were produced by GPS and with Y_2O_3 as the only sintering additive. The influence of a post-sintering heat treatment on the high temperature properties of the GPS materials was of special interest. The properties of these materials are compared with those of a Si_3N_4/SiC nanocomposite prepared by HP that was studied previously in our laboratory.[12] This HP reference material was shown to exhibit excellent mechanical high temperature properties. Additionally the results of this work are compared with data published for other silicon nitride materials prepared by GPS.

2. Experimental details

2.1. Materials

All materials investigated in this study were fabricated at the Fraunhofer Institute IKTS, Dresden, Germany. Starting powders and their characteristics are listed in Table 1. The main constituent of the material was a commercial high purity α-Si_3N_4 powder (SN E-10, Ube Industries, Yamaguchi, Japan). As the SiC source two different powders were used, (i) a commercial grade α-SiC powder (UF15, H.C. Starck, Goslar, Germany), called type "SCu" and (ii) an amorphous SiCN powder (~80% SiC) produced by plasma chemical synthesis, called type "SCp". The fabrication of the SiCN powder (Institute of Inorganic Chemistry, Academy of Science of Latvia, Riga, Latvia) has been described elsewhere.[13] Y_2O_3 (grade fine, H.C. Starck, Goslar, Germany) was applied as a densification aid.

The starting powder mixture contained 10 wt.% Y_2O_3 in the case of the HP material and 12 wt.% for the GPS materials. The higher content of the sintering additive in the GPS material was necessary to achieve a nearly dense material. Homogeneous mixtures of the starting powders were obtained by milling in isopropanol in a planetary mill. After drying and calcinating at 450 °C for 1 h, the powder mixtures were isostatically pressed into rectangular blocks of the dimensions 25×25×60 mm and gas pressure sintered. Details of the fabrication process are described elsewhere.[6] The same starting powders and mixing conditions were used to fabricate the HP material.[12]

In Fig. 1 both the GPS and HP densification routes are compared. For the GPS cycle a higher maximum sintering temperature (GPS: 1900 °C/HP: 1840 °C) and a longer dwell time (GPS: 2 h/HP: 1 h) had to be selected to allow a nearly complete densification. Along both densification routes a nitrogen pressure was applied to avoid decomposition of the Si_3N_4. Due to the higher sintering temperature during GPS a nitrogen pressure of 6 MPa was chosen for this process. Thermodynamic calculations [6] showed that GPS materials of maximum density and minimum weight loss (due to decomposition of the liquid phase) are obtained under the chosen nitrogen pressure. For the HP material a nitrogen pressure of 0.1 MPa was sufficient. In both cases, however, the gas pressure did not contribute to the densification. The mechanical pressure applied during HP was 30 MPa. Owing to the fast cooling rate at the end of the GPS cycle and to the enhanced amount of sintering additives it was supposed that the materials contained a substantial amount of amorphous phase. To promote crystallisation a post-sintering heat treatment in N_2-atmosphere was carried out at 1400 °C for 24 h on some specimens. In Table 2 the designations and compositions of the materials as well as the heat treatment parameters are summarised.

2.2. Mechanical testing

For testing the mechanical properties rectangular bars of the dimensions 3×4×50 mm were cut from the sintered or hot-pressed billets. All specimens were ground with a 15 μm diamond wheel before testing. Edges were chamfered to eliminate machining defects.

Table 1
Properties of the starting powders

Powder	Phase content	BET-surface area (m^2/g)	Oxygen content (wt.%)	Main impurities (ppm)
SN E-10	96% α-Si_3N_4 4% β-Si_3N_4	10.4	1.6	Cl < 100, Fe < 100, Ca, Al < 50
SiCN (type "p")	β-SiC, Partially amorphous	10.4	0.8	F70, Free Si 5000
UF-15 (type "u")	α-SiC	~15	1.5	Al 300, Ca 100, Fe 500
Y_2O_3	Y_2O_3	12.2		Al 50, Ca 30, Fe 50

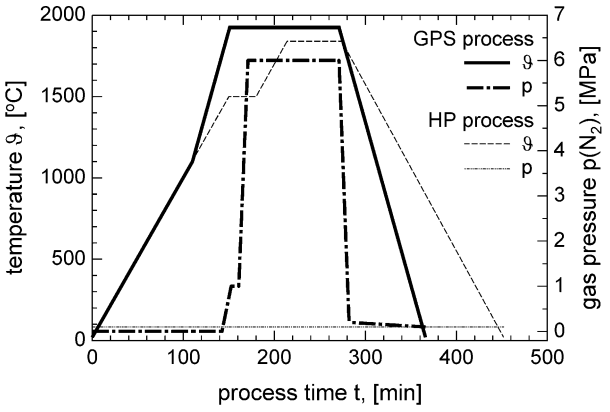

Fig. 1. Temperature and nitrogen pressure as a function of process time for both the GPS and the HP cycle.

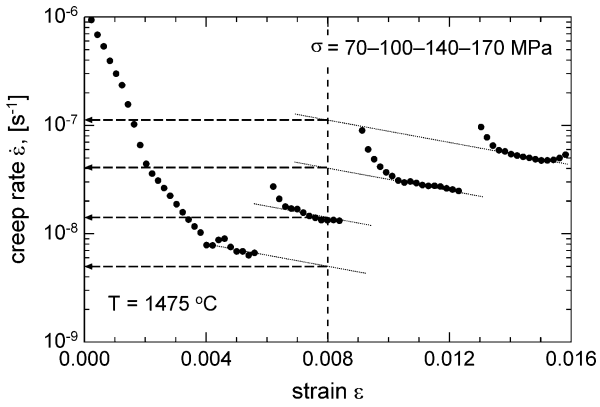

Fig. 2. Typical creep rate vs. strain curve of a stress change test and determination of quasi-stationary creep rates for further analysis.

Creep tests were performed in four-point bending using a fixture made of silicon carbide with inner and outer span length of 20 and 40 mm, respectively. The measurements were carried out in a dead-weight creep machine in air atmosphere at temperatures between 1450 and 1600 °C with outer fibre stresses in the range from 70 to 300 MPa. The sample deflection was recorded continuously during the creep test. From the deflection data, the outer fibre strain was calculated as a function of time, t, by the method of Hollenberg et al. [14] and taken as the creep strain, ε. The creep rate, $\dot{\varepsilon}$, was calculated from the slope of the ε vs. t curve. The accuracy of the deflection measurement permitted the determination of creep rates down to a level of $2{\cdot}10^{-9}$ s^{-1}.

The steady-state creep rate, $\dot{\varepsilon}_s$, is usually described by the Norton equation: [15]

$$\dot{\varepsilon}_s = A{\cdot}\sigma^n{\cdot}\frac{1}{d^m}{\cdot}\exp\left(-\frac{Q_c}{RT}\right) \quad (1)$$

where A is a constant, depending on the respective material and on its microstructure, σ is the stress, n is the stress exponent, d is the grain size, m is the grain size exponent, Q_c is the activation energy for creep, and T and R have their usual meaning.

Stress and temperature change tests were carried out to determine n and Q_c, respectively. In some tests steady-state creep behaviour was not really achieved. In these cases quasi-stationary creep rates were defined as shown in Fig. 2. Here the measured creep rate is plotted as a function of strain for a stress change test. For each stress a range of the $\dot{\varepsilon}$ vs. ε curve was observed with a constant (negative) slope. Each range was then extrapolated to the same strain of $\varepsilon = 0.008$ as demonstrated by the dotted lines. These extrapolated creep rates (see arrows) were used for further analysis.

Temperature change tests were performed on one sample of each grade with a constant stress of 100 MPa at temperatures between 1450 and 1600 °C. The temperature was increased/decreased in steps of 25 °C after reaching a steady-state or quasi-stationary creep rate. In a similar way stress change tests were carried out at a temperature of 1475 °C and stresses between 70 and 300 MPa. This temperature level was necessary to achieve creep rates above the detection limit even at the lowest stress.

Stress rupture tests were carried out at 1400 °C to study the lifetime under creep conditions. GPS and HP materials were tested at 180–250 and 500–600 MPa, respectively, to cause failure within a reasonable time scale. At the moment of failure, the values of failure time, t_f, failure strain, ε_f, and the minimum creep rate, $\dot{\varepsilon}_{min}$, were taken.

Strength data were measured in 4-point bending with inner and outer span length of 20 and 40 mm, respectively, according to DIN EN843/DIN 51110 part 2 at

Table 2
Designations of the materials, their compositions and post-sintering heat treatment conditions

Material	Additive content (wt.% Y_2O_3)	SiC particles		Crystallisation heat treatment
		Type	Content (wt.%)	
12YG25SCp	12	P	25	Non
12YG25SCpc	12	P	25	1400 °C/24 h
12YG25SCu	12	U	25	Non
12YG25SCuc	12	U	25	1400 °C/24 h
10YH10SCp[a]	10	P	10	–

[a] Reference material densified by hot-pressing.[6]

the Fraunhofer Institute IKTS, Dresden, Germany. Flexural strength test were done at room temperature in air and at 1400 °C in vacuo with a crosshead speed of 0.5 mm/min using a universal testing machine. Each data point presents the mean value of at least five single tests.

2.3. Microstructural characterisation

The microstructure of the GPS materials was characterised by X-ray diffractometry (XRD) and scanning electron microscopy (SEM).

XRD analyses were carried out using a Philips PW1729 powder diffractometer equipped with a CuK_α radiation source. Both as-sintered and heat-treated specimens as well as crept samples were analysed in the solid form on ground surfaces. Analysis of the diffraction patterns was performed by comparison with the data listed in the library of reference spectra of the Joint Committee on Powder Diffraction Standards (JCPDS).

Polished and plasma-etched (SF_6) sections of the bulk materials were examined in a Leo Gemini 1530 scanning electron microscope. To prevent surface charging during examination specimens were coated with a thin layer of gold. In Figs. 3a and b typical microstructures of the as-sintered GPS materials 12YG25SCp and 12YG25SCu are shown. The dark hexagonal and elongated areas are Si_3N_4 grains, bright areas characterise the grain-boundary phase, and grey areas consist of SiC particles and grain-boundary phase. It is difficult to distinguish between SiC particles and grain-boundary phase because both are affected similarly by plasma etching. The microstructure of the two different GPS materials was found to be very similar and independent of the type of the SiC powder added. Except for very few large Si_3N_4 grains their diameter is in a range of about 0.1–2 μm. Bright dots within larger Si_3N_4 grains are small intragranular SiC particles with a size up to about 200 nm. Most of the SiC particles are located at the grain boundaries.

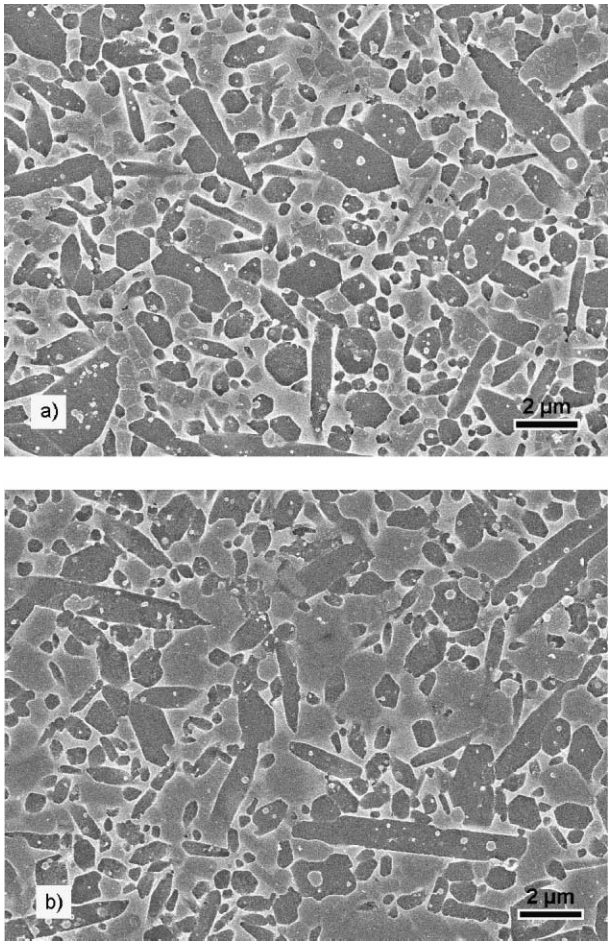

Fig. 3. Microstructure of the GPS materials (a) 12YG25SCp and (b) 12YG25SCu (dark—Si_3N_4 grains, bright—grain-boundary phase, grey—SiC + grain-boundary phase).

3. Results

Typical creep curves (strain ε vs. time t) of as-sintered and heat-treated GPS materials are shown in Fig. 4. The creep behaviour of both materials is characterised by primary creep followed by pronounced steady-state creep. The accumulated creep deformation is larger for the as-sintered material 12YG25SCp than for the heat-treated material 12YG25SCpc. The same applies to the creep rates. This can also be seen in Fig. 5. Here, steady-state creep rates measured in temperature change tests are plotted as a function of temperature.

Material 12YG25SCp shows somewhat lower creep rates than material 12YG25SCu. This is a minor but significant effect. Data of the hot-pressed reference

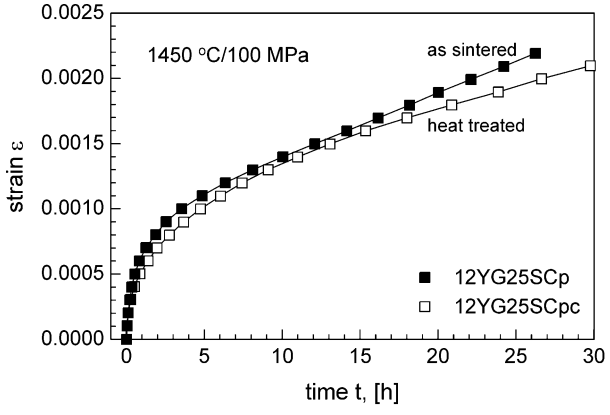

Fig. 4. Typical creep curves ε vs. t measured at 1450 °C/100 MPa for the as-sintered and the heat-treated GPS materials 12YG25SCp and 12YG25SCpc, respectively.

material 10YH10SCp are also plotted in Fig. 5 for comparison. The difference in creep rate compared to the as-sintered GPS materials is about one order of magnitude. To improve the creep resistance of the GPS material the amorphous grain-boundary phase was crystallised by annealing at 1400 °C for 24 h. The creep rates

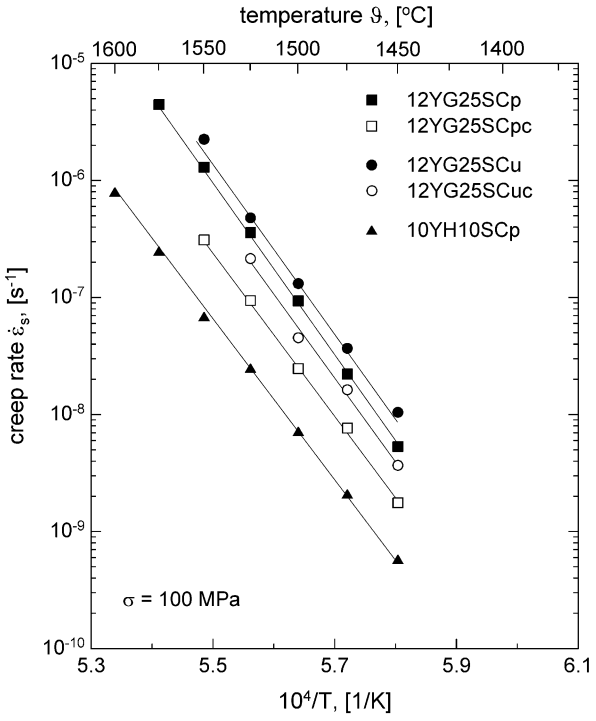

Fig. 5. Steady-state creep rate as a function of temperature at a stress of 100 MPa.

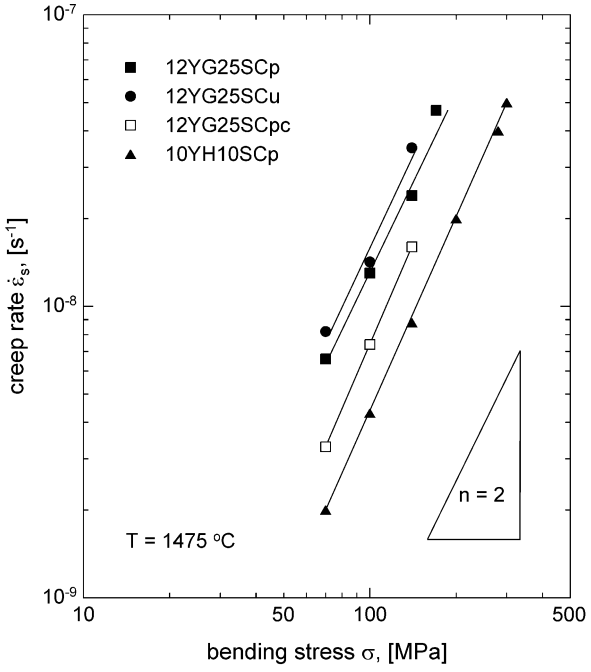

Fig. 6. Steady-state or quasi-stationary creep rate as a function of stress at a temperature of 1475 °C.

measured for the heat-treated material 12YG25SCpc are between those of the HP reference material and the as-sintered GPS material. In fact, the creep resistance of 12YG25SCp increased remarkably due to the annealing by a factor of about six. The heat treatment affected also the creep properties of 12YG25SCu. Creep rates of the annealed material 12YG25SCuc were lower by a factor of about four compared to those of the as-sintered material, but higher than for 12YG25SCpc.

The activation energy for creep was calculated from the slope of the straight lines in Fig. 5 according to Eq. (1). The results are summarised in Table 3. For all materials the activation energy is very high with values between 1290 and 1440 kJ/mol. There was no systematic variation with the SiC-type or the thermal treatment.

In Fig. 6 steady-state or quasi-stationary creep rates measured at 1475 °C in the stress change tests are plotted as a function of the bending stress. For all materials the stress dependence of the creep rates could be approximated by straight lines. According to Eq. (1) the slope of these lines is the stress exponent, n, which was found to be between 1.9 and 2.2 (Table 3) for the various materials.

Table 3
Parameters determined in creep and stress rupture tests

Material	Q_c (kJ/mol)	n	n*	σ_t (MPa)	N
12YG25SCp	1420	1.9	31	172	39
12YG25SCu	1445	2.1	32	168	45
12YG25SCpc	1340	2.2	41	200	78
12YG25SCuc	1055	–	–	–	–
10YH10SCp	1290	2.2	40	505	82

To compare the creep data generated in the stress change tests with those of the stress rupture experiments performed at 1400 °C the former were normalised to 1400 °C by means of Eq. (1) taking the activation energy for creep of the respective material (Table 3). These converted creep rates are plotted in Fig. 7 together with the minimum creep rates obtained at 1400 °C in the stress rupture tests. Two different types of behaviour are observed. At low and intermediate stresses stationary creep rates were obtained and their stress dependencies are described by the stress exponents, n, summarised in Table 3. Above a certain stress, samples failed due to cracking before reaching the steady-state creep regime. Hence, only minimum creep rates were obtained which are presented by the data points in the high stress region. These data can also be approximated by straight lines. Their slope is very steep and gives apparent stress exponents, n*, between 30 and 40 (Table 3). The GPS materials 12YG25SCp and 12YG25SCu show no difference in the high stress region. The effect of annealing on the minimum creep rates is negligible as presented by the data points for material 12YG25SCpc.

The two different stress dependencies meet in an intersection point, which can be defined as a characteristic transition stress, σ_t. Its value was found to depend on the type of the material and is listed in Table 3. Below σ_t, the mechanical behaviour is described by the absence of failure within a test duration of up to 200 h and a large bulk deformation exceeding 1%. Above σ_t,

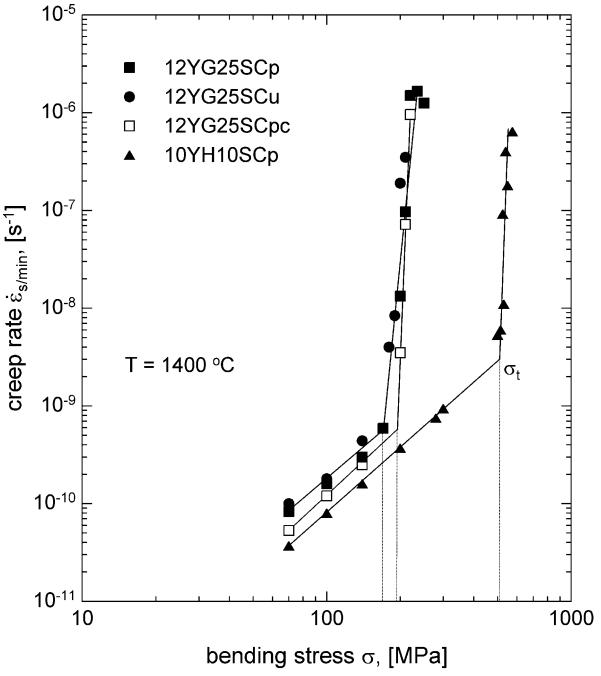

Fig. 7. Creep rates measured in stress change tests and stress rupture experiments as a function of stress at a temperature of 1400 °C.

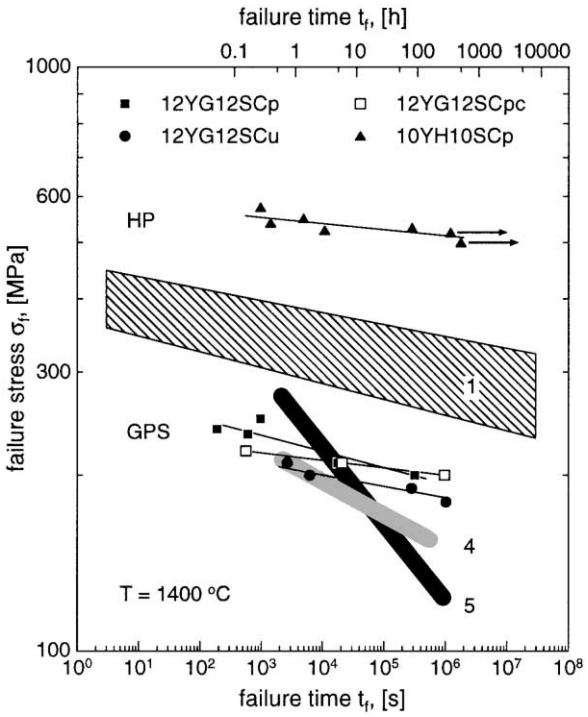

Fig. 8. Flexural stress rupture data for the materials of this study at 1400 °C and data taken from the literature—1: $7BeSiN_2 7SiO_2$, 1200 °C, 4-point bending[18]; 4: GR1 (Kyocera), 1400 °C, tension[23]; 5: SN88M (NGK), 1400 °C, tension.[23].

the mechanical response is characterised by a very strong stress dependence of the creep rate and a short lifetime. For the as-sintered GPS materials comparable σ_t values of 170 MPa were obtained. Annealing seems to slightly increase σ_t to about 200 MPa. However, for the HP material a distinct higher value of 505 MPa was found.

In Fig. 8 the results of the stress rupture tests performed at 1400 °C are plotted as failure stress, σ_f, vs. failure time, t_f. Failure of ceramics at high temperature is controlled either by subcritical crack growth (SCG) or by creep damage accumulation. High values of n^* as calculated from the data in the high stress range in Fig. 7 as well as failure after relatively short times and before reaching a stationary creep rate suggest failure due to SCG. In Ref. 16 a relationship was derived for t_f under static loading conditions:

$$t_f = B \cdot \frac{S_I^{N-2}}{\sigma_f^N} \quad (2)$$

where S_I is the inert strength of the material, σ_f is the failure stress, N is the crack growth exponent, and B is an abbreviation for $B = 2/\{A\ Y^2(N\text{-}2)\ K_{Ic}^{N-2}\}$ with Y the stress intensity calibration of fracture mechanics and K_{Ic} the fracture toughness. According to Eq. (2) the stress rupture data of each material were approximated by a straight line in the log σ_f vs. log t_f plot of Fig. 8 with the slope $-1/N$. The exponent N is a measure of the resistance against SCG, the higher N the less the material is prone to SCG. The as-sintered GPS materials are characterised by a relatively small N of 39 or 45, whereas the annealed sample and the HP reference material show higher values of 78 and 82, respectively (see Table 3). Obviously the annealing treatment leads to an increase in crack growth resistance. Nevertheless, for the GPS materials the stress level where SCG occurs is much lower than for the HP material. The annealing of the GPS material has no effect on this level (Fig. 8).

In Table 4 strength data are summarised, of the materials tested in this work, as well as of other GPS materials published in the literature. At room temperature material 12YG25SCu has a significantly higher flexural strength than material 12YG25SCp. However, at high temperatures the strength of 12YG25SCu decreases drastically, whereas the decrease in strength for material 12YG25SCp is less pronounced. Thus, the retained strength (ratio σ_{HT}/σ_{RT}) differs by a factor of two between both GPS materials. For annealed samples no strength data were available. Flexural strength at RT for the HP reference material is comparable with that for 12YG25SCu.

4. Discussion

Based on the results presented before the following findings can be summarised:

(i) GPS materials creep faster than the HP reference material,

Table 4
Room temperature (RT) and high temperature (HT) strength data of various GPS materials and the HP reference material

Material/additives[a]	RT (σ_{RT})	Strength σ (MPa) at HT (σ_{HT})	Retained strength (σ_{HT}/σ_{RT})	Method	Ref.
12YG25SCp	645	430 (1400 °C)	0.67	4-Point bending	This work
12YG25Scu	840	320 (1400 °C)	0.38	4-Point bending	This work
10YH10SCp	830	–	–	4-Point bending	This work
10Y5A	814±97	–	–	4-Point bending	17
10Y5A10SC	651±80	–	–	4-Point bending	17
5.5Y3A1.5AlN	323–855[b]	–	–	3-Point bending	9
5.5Y3A1.5AlN5SC	508–644[b]	–	–	3-Point bending	9
5.5Y3A1.5AlN7SC	497–634[b]	–	–	3-Point bending	9
5.5Y3A1.5AlN10SC	166–399[b]	–	–	3-Point bending	9
5.5Y3A	910	–	–	3-Point bending	5
5.5Y3A5SC	955–1010[c]	–	–	3-Point bending	5
$7BeSiN_2 7SiO_2$	560±68	490 (1400 °C)	0.88	3-Point bending	18
6Y2A	542±37–817±62[b]	–	–	4-Point bending	19
$Sr_2La_4Yb_4(SiO_4)_6O_2$	362±38–607±160[b]	–	–	4-Point bending	19
10Y0A–0Y10A	788–1304[d]	460–1063[d] (1000 °C)	0.39–0.85[d]	4-Point bending	20
5Y3A1M	1600	1100 (1200 °C)	0.69	No details	21
5Y3A	1220	600 (1200 °C)	0.49	No details	21
5Y3.5M	860	780 (1200 °C)	0.91	No details	21
ST-1 (NGK)	1085	480 (1400 °C)	0.44	4-Point bending	22
GR-1 (Kyocera)	809±17	580 (1400 °C)	0.72	4-Point bending	23
SN88M (NGK)	856±21	640 (1400 °C)	0.75	4-Point bending	23

[a] $Y = Y_2O_3$, $A = Al_2O_3$, M = MgO, SC = SiC, number in front of the letter(s) gives the content in wt.%.
[b] Depending on densification conditions.
[c] Depending on SiC-powder type.
[d] Depending on composition.

(ii) a heat treatment causes a distinct reduction of the creep rates of GPS materials,
(iii) material 12YG25SCu creeps faster than material 12YG25SCp,
(iv) GPS materials show premature failure due to cracking at smaller loads than the HP reference material, and
(v) GPS materials are less resistant against SCG than the HP material.

Comparing 12YG25SCp with 10YH10SCp reveals that the GPS material contains more sintering additive (yttria) and silicon carbide particles than the HP material. For hot-pressed materials it has been shown previously[24] that the increase of the yttria content from 10 to 12 wt.% and that of the SiC particles from 10 to 25% causes a rise of the creep rate by a factor of approximately 1.3 and 3, respectively. Therefore, the different compositions of GPS and HP materials are responsible for part of the difference in the creep resistance. On the other hand, HP materials are known to have a very small grain size ($\bar{d} << 1\mu m$ [6]), whereas that of the GPS materials is rather large ($\bar{d} \sim 1\mu m$, Fig. 3). According to Eq. (1) a larger grain size results in a reduction of the creep rate leading to a smaller difference between GPS and HP materials. However, the observed difference in creep rate of about one order of magnitude (Fig. 5) is larger than the difference caused by the composition. Hence, a further effect has to be considered, namely, the degree of crystallisation of the glassy phase. The fast cooling at the end of the GPS cycle (Fig. 1) is expected to give rise to incomplete crystallisation of the glassy phase. The presence of even very thin amorphous grain-boundary films is well known to deteriorate the creep resistance.[25] The amount of the intergranular glassy phase, however, is too small to be detected by XRD. As shown in Fig. 9 only crystalline secondary phases like the J-phase ($Y_8Si_4N4O_{14}$) and the K-phase ($YNSiO_2$) were identified in the as-sintered GPS materials.

The heat treatment as well as the annealing during the creep test only caused minor changes in type and amount of the crystalline secondary phases. As Fig. 9 shows, the amount of the K- and H-phase was found to increase and that of the J-phase to decrease. Such small effects are not expected to significantly alter the creep behaviour.

Consequently, the reduction of the creep rate of the annealed GPS materials by a factor of 6 is attributed to the crystallisation of the intergranular glassy phase present in the as-sintered material due to the heat treatment. For a GPS material doped with $BeSiN_2$ and SiO_2 [18] there was also found a reduction of the creep rate by a factor of 6 due to a heat treatment which caused crystallisation of the intergranular glassy phase.

The slightly lower creep resistance of material 12YG25SCu compared to that of material 12YG25SCp

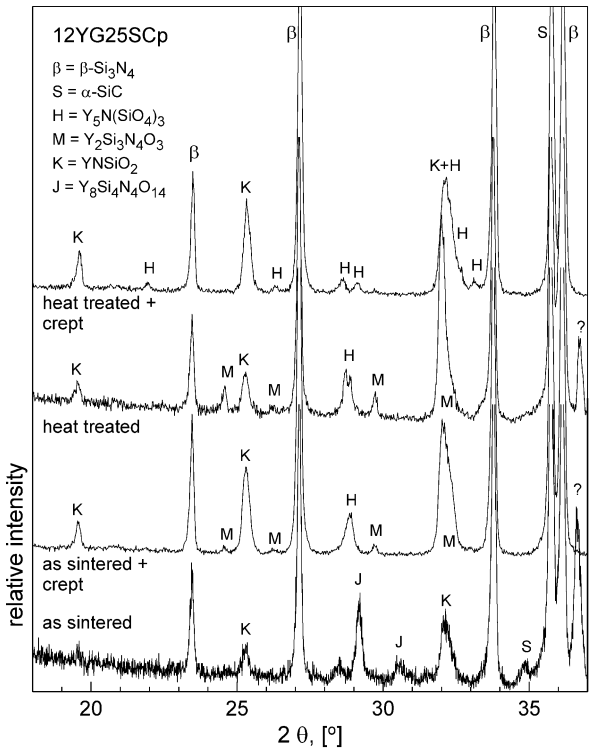

Fig. 9. X-ray diffraction pattern of material 12YG25SCp after different annealing treatments.

can be explained by differences in impurity content (Table 1). Powder SCu contains small amounts of Ca and Al as impurities which are known to reduce the viscosity of silica glass[26] and, therefore, the creep resistance.[24] Furthermore, the Ca and Al impurities in material 12YG25SCu are thought to be responsible for the low retained strength found at 1400 °C (Table 4). The strength data measured for the materials of this study are comparable to those found for other GPS materials. The data summarised in Table 4 display a wide scatter and illustrate that strength very much depends on densification conditions and material composition, both affecting the microstructure. Furthermore, differences in loading geometry and specimen size have to be considered so that further conclusions cannot be drawn.

Creep lifetime is controlled either by creep damage accumulation or by SCG. If lifetime is controlled by creep damage accumulation then the Monkman–Grant relation [27]—$\dot{\varepsilon}_{s,min} \cdot t_f = \text{const.}$— should be valid and the failure strain ε_f should be essentially independent of stress. For the GPS materials of this study, however, the contrary has been found. The product of minimum creep rate times failure time is not a constant (variation between 0.0008 and 0.0042) and the failure strain strongly decreases with increasing stress, from $\varepsilon_f \sim 0.01$ at 200 MPa to $\varepsilon_f \sim 0.002$ at 230 MPa. Hence, failure at stresses above σ_t is caused by SCG and the analysis of the stress rupture data by Eq. (2) is adequate. The data for the SCG exponent N (Table 3) obtained from the slope of the lines in Fig. 8 suggest that the resistance against SCG of the as-sintered GPS materials is lower than that of the HP material. This is attributed to the presence of an intergranular glassy phase which provides a path for easy crack propagation. If this glassy phase crystallises due to the heat treatment (12YG25SCpc) the resistance against SCG increases and becomes comparable to that of the HP material. Simultaneously the transition stress, σ_t, above which failure occurs, is slightly increased. For material 12YG25SCpc, however, σ_t is still smaller than for the HP reference material. This can be explained by different defect populations in the GPS and HP materials, as the following consideration shows. GPS materials are characterised by a larger grain size than HP materials and additionally contain some larger pores due to imperfect densification. Furthermore, it can be assumed that SCG starts from the largest defect when the stress intensity K_I at this defect exceeds a threshold value $K_{I,t}$. $K_{I,t}$ is a material constant valid for SCG at elevated temperatures.[28] It is assumed here that $K_{I,t}$ is the same for GPS and HP materials. From the basic equation of linear elastic fracture mechanics

$$K_I = Y \cdot \sigma \cdot a^{1/2} \tag{3}$$

it follows that the stress at which crack propagation starts depends on the defect size a. The different values of σ_t found in Fig. 7 indicate that the largest defects in the GPS materials are approximately 6 times larger than those in the HP material. This result is very reasonable.

Stress rupture data measured at elevated temperature are rare to find for other GPS materials and comparison with the results of this study is difficult since different conditions of temperature or loading were applied. In Fig. 8 data are shown for an experimental GPS material doped with $BeSiN_2$ and silica and tested at 1200 °C in 4-point bending[18] and two commercial materials tested at 1400 °C in tension.[23] Taking into account that the stress necessary for SCG increases with decreasing temperature and that ceramics are more susceptible to crack growth under tensile loading than in bending leads to the conclusion that the GPS materials of this study show no extraordinary stress rupture behaviour.

Finally, the creep behaviour of the GPS materials of this study is compared with that of other GPS materials. As can be seen in Fig. 10, the materials of this study were creep-tested at temperatures higher than in all other studies found in the literature. This is attributed to the fact that the creep rates at 1400 °C/100 MPa are below the detection limit of the test facilities used in this study and are the lowest creep rates reported for silicon nitride materials densified by GPS so far. The material doped with $BeSiN_2$ and silica[18] (No. 1, Fig. 10) creeps about 6 times faster than the as-sintered materials of

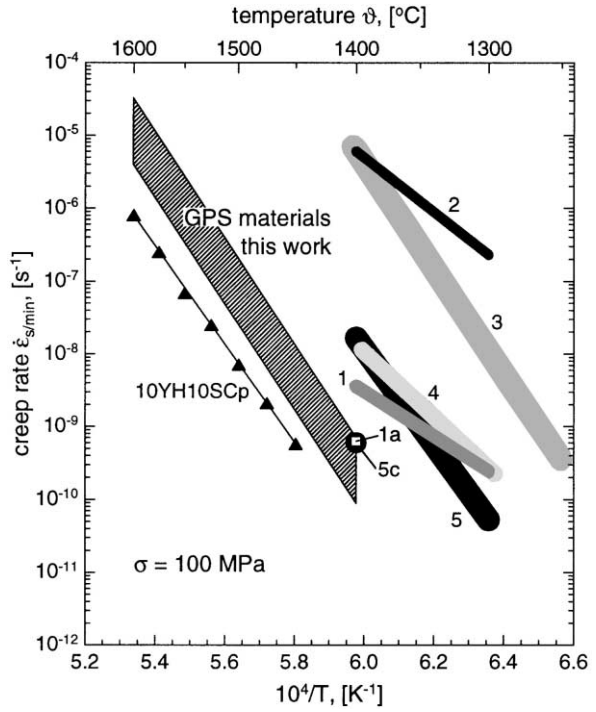

Fig. 10. Comparison of the creep behaviour of the materials of this study with that of other GPS materials (1: $7BeSiN_2 7SiO_2$, 3-point bending;[18] 1a: 1, annealed 1600 °C/N_2/16 h;[18] 2: 6Y2A, 4-point bending;[29] 3: ST-1 (NGK), tension;[22] 4: GR1 (Kyocera), tension;[23] 5: SN88M (NGK), tension;[23] 5c: 5, compression[23]).

this study. Only the creep rate of the heat-treated version of this material is comparable with that measured for the as-sintered materials in this study. If yttria ***and*** alumina are used simultaneously as densification aids the creep resistance is reduced by about 4 orders of magnitude (6Y2A—No. 2, Fig. 10). A direct comparison of the materials of this study with the commercial silicon nitride ceramics ST-1 and SN88M (NGK Insulator Co., Ltd., Nagoya, Japan; Nos. 3 and 5, Fig. 10) and GR1 (Kyocera, Kyoto, Japan; No. 4, Fig. 10) is not possible since these materials were tested in tension. However, considering the effect of loading conditions (tension–bending–compression) on creep rate as demonstrated by the data for SN88M (Fig. 10, No. 5—tension, No. 5c—compression) reveals that all three commercial materials creep faster than the GPS materials investigated in this study.

5. Conclusions

The GPS technology proved to be a suitable means to fabricate Si_3N_4/SiC nanocomposites with advanced mechanical properties. However, the creep resistance of such ceramics is lower than that of HP materials due to imperfect crystallisation of the intergranular phase. By means of a post-sintering heat treatment (crystallisation treatment) the creep resistance can be improved and becomes comparable with that of optimised HP materials. Hence, the cooling regime of the GPS cycle has to be modified or a post-densification treatment has to be applied to obtain materials with improved creep resistance. Simultaneously, the resistance against SCG is increased. But, due to the rather coarse microstructure of the GPS materials, stress rupture occurs already at stresses as low as 170 MPa leading to short lifetimes at slightly higher loads. This turns out to be a limitation for the application of GPS materials. However, the analysis of all available creep data in the literature reveals that the materials tested in this study belong to the most creep resistant silicon nitride ceramics prepared by GPS. Under consideration that the GPS technology is less cost intensive than HP or HIPing and allows the production of complex shaped bodies the results of this study demonstrate the potential of Si_3N_4/SiC nanocomposite materials for industrial applications where a high strength is not the limitation.

Acknowledgements

The authors thank Dr. M. Herrmann and Dr. H. Klemm from IKTS Dresden, Germany, for the preparation of the materials and the measurement of the strength data. Financial support by the German Research Council (DFG), reference number Hu 215/7, is gratefully acknowledged.

References

1. Niihara, K., New design concept of structural ceramics—ceramic nanocomposites. *J. Ceram. Soc. Jpn*., 1991, **99**, 974–982.
2. Hirano, T., Niihara, K., Ohji, T. and Wakai, F., Improved creep resistance of Si_3N_4/SiC nanocomposites fabricated from amorphous Si–C–N precursor powder. *J. Mater. Sci. Lett*., 1996, **15**, 505–507.
3. Pezzotti, G. and Sakai, M., Effect of a silicon carbide 'nano-dispersion' on the mechanical properties of silicon nitride. *J. Am. Ceram. Soc*., 1994, **77**, 3039–3041.
4. Rendtel, A., Hübner, H., Herrmann, M. and Schubert, Ch., Si_3N_4/SiC nanocomposite materials: II, hot strength, creep, and oxidation resistance. *J. Am. Ceram. Soc*., 1998, **81**, 1109–1120.
5. Kennedy, T., Poorteman, M., Cambier, F. and Hampshire, S., Silicon nitride– silicon carbide nanocomposites prepared by water processing of commercially available powders. *J. Eur. Ceram. Soc*., 1997, **17**, 1917–1923.
6. Herrmann, M., Schubert, Ch., Rendtel, A. and Hübner, H., Si_3N_4/SiC nanocomposite materials: I, fabrication and mechanical properties at room temperature. *J. Am. Ceram. Soc*., 1998, **81**, 1095–1108.
7. Klemm, H., Herrmann, M. and Schubert, Ch., High-temperature properties of Si_3N_4/SiC nanocomposites. *Ceram. Eng. Sci. Proc*., 2000, **21**, 3–713–720.
8. Greil, P., Petzow, G. and Tanaka, H., Sintering and HIPing of silicon nitride-silicon carbide composite materials. *Ceram. Int*., 1987, **13**, 19–25.
9. Kennedy, T., O'Neil, J. P. and Hampshire, S., Densification and properties of Si_3N_4/SiC nanocomposites. *Silicates Ind*., 1996, **61**, 201–205.

10. Bernhard-Granger, G., Crampon, J., Duclos, R. and Cales, B., Glassy grain-boundary phase crystallisation of silicon nitride: kinetics and phase development. *J. Mater. Sci. Lett.*, 1995, **14**, 1362–1365.
11. Pullum, O. J. and Lewis, M. H., The effect of process atmosphere on the intergranular phase in silicon nitride ceramics. *J. Eur. Ceram. Soc.*, 1996, **16**, 1271–1275.
12. Rendtel, P., Rendtel, A., Hübner, H., Klemm, H. and Herrmann, M., Effect of long-term oxidation on creep and failure of Si_3N_4 and Si_3N_4/SiC nanocomposites. *J. Eur. Ceram. Soc.*, 1999, **19**, 217–226.
13. Zalite, I., Boden, G., Schubert, Ch., Lodzina, A., Plitmanis, J. and Miller, T., Sintering of fine silicon nitride powders. *Latv. Chem. J.*, 1992, **2**, 152–159.
14. Hollenberg, G. W., Terwilliger, G. R. and Gordon, R. S., Calculation of stresses and strains in four-point bending creep tests. *J. Am. Ceram. Soc.*, 1971, **54**, 196–199.
15. Norton, F. H., The flow of ceramic bodies at elevated temperatures. *J. Am. Ceram. Soc.*, 1936, **19**, 129–134.
16. Davidge, R. W., MacLaren, J. R. and Tappin, G., Strength-probability-time (SPT) relationship in ceramics. *J. Mater. Sci.*, 1973, **8**, 1699–1705.
17. Akimune, Y., Hirosaki, N. and Ogasawara, T., Mechanical properties and microstructure in sintered and HIPed SiC particle/Si_3N_4 composites. *J. Mater. Sci.*, 1992, **27**, 6017–6021.
18. Greskovich, C., Pasco, W. D. and Quinn, G. D., Thermomechanical properties of a new composition of sintered Si_3N_4. *Am. Ceram. Soc. Bull.*, 1984, **63**, 1165–1170.
19. Tiegs, T. N., Nunn, S. D., Beavers, T. M., Menchhofer, P. A., Barker, D. L. and Coffey, D. W., Gas pressure sintering of silicon nitride to optimize fracture toughness. *Ceram. Eng. Sci. Proc.*, 1995, **16**(4), 467–473.
20. Riedel, G., Bestgen, H. and Herrmann, M., Influence of sintering additives with differing proportions of Y_2O_3/Al_2O_3 on the sintering and material properties of Si_3N_4 ceramics. *cfi/Ber. DKG*, 1998, **75**(10), 30–34.
21. Kondo, N., Wakai, F., Yamagiwa, M., Nishioka, T. and Yamakawa, A., High temperature deformation of silicon nitride ceramics with different microstructures. *Mater. Sci. Eng.*, 1996, **A206**, 45–48.
22. Lofaj, F., Usami, H., Ikeda, Y., Mizuta, Y. and Kawamoto, H., Creep fracture behavior of gas pressure sintered silicon nitride by X-ray CT. In *Proc. of Yokohama Intern. Gas Turbine Congress*. Gas Turbine Society of Japan, Tokyo, Japan, 1995, pp. 37–44.
23. Lofaj, F., Cao, J.-W., Okada, A. and Kawamoto, H., Comparison of creep behavior and creep demage mechanisms in the high-performance silicon nitrides. In *Proc. 6th Int. Symp. on Ceramic Materials and Components for Engines*, ed. K. Niihara, S. Hirano, S. Kanzaki, K. Komeya and K. Morinaga. Technoplote Co Ltd, Tokyo, 1998, pp. 713–718.
24. Rendtel, A. and Hübner, H., Creep resistant silicon nitride ceramics- approaches of microstructural design. *Ceram. Eng. Sci. Proc.*, 2000, **21**(4), 515–526.
25. Pharr, G. M. and Ashby, M. F., On creep enhanced by a liquid phase. *Acta Metall.*, 1983, **31**, 129–138.
26. Pezzotti, G., Grain-boundary viscosity of calcium-doped silicon nitride. *J. Am. Ceram. Soc.*, 1998, **81**, 2164–2168.
27. Monkman, F. C. and Grant, N. J., An empirical relationship between rupture life and minimum creep rate in creep rupture tests. *Proc. Am. Soc. Test. Mater.*, 1956, **56**, 593–620.
28. Foley, M. R. and Tressler, R. E., Threshold stress intensity for crack growth at elevated temperatures in a silicon nitride ceramic. *Adv. Ceram. Mater.*, 1988, **3**, 382–386.
29. Todd, J. A. and Xu, Z. Y., The high-temperature creep deformation of Si_3N_4–$6Y_2O_3$–$2Al_2O_3$. *J. Mater. Sci.*, 1989, **24**, 4443–4452.